PHYSICAL REVIEW B **68**, 144201 (2003)

Glass-forming ability determined by an *n*-body potential in a highly immiscible Cu-W system through molecular dynamics simulations

H. R. Gong, L. T. Kong, W. S. Lai, and B. X. Liu*

Advanced Materials Laboratory, Department of Materials Science and Engineering, Tsinghua University, Beijing 100084, China

(Received 20 October 2002; revised manuscript received 21 January 2003; published 7 October 2003)

With an important aid from *ab initio* calculations, an *n*-body potential is constructed under the embedded atom method for a highly immiscible Cu-W system characterized by a positive heat of formation of +33 kJ/mol. The obtained potential is capable of reproducing some realistic physical properties, such as cohesive energies and lattice constants, etc., of Cu and W, as well as two nonequilibrium Cu_3W and CuW compounds. Applying the potential, molecular dynamics simulations using solid solution models are conducted to calculate the critical solid solubility, at which a metallic glass transition takes place, thus determining the glass-forming range of the Cu-W system to be from 20 to 65 at. % of W, which is in good agreement with the experimental results. Interestingly, an abnormally large volume expansion in association with the transition is found to be within 6.9–13.1% in the Cu-W system and it is much greater than the typical value of 1–2% frequently observed in the systems with negative heats of formation.

DOI: 10.1103/PhysRevB.68.144201 PACS number(s): 64.60.Cn, 61.43.Dq, 82.20.Wt

I. INTRODUCTION

During the last two decades, several empirical models have appeared to predict the glass-forming ability (GFA) or glass-forming range (GFR) favoring the formation of amorphous alloys of a binary metal system. Liu *et al.* proposed a structural difference rule which predicted that an amorphous phase would most likely be formed in binary metal systems, which consist of two constituent metals of different crystalline structures, at an overall composition located in the middle of the two-phase region of the equilibrium phase diagram.[1] Meanwhile, Alonso and Simozar proposed constructing a two-dimensional map for predicting a GFA with two parameters, i.e., the ratio of atomic radii of the metals *A* and *B* and the heat of formation (ΔH_f) calculated by Miedema's model at an equiatomic stoichiometry.[2] Based on comprehensive experimental studies, Liu *et al.* proposed, a little later, an empirical model on the basis of two intrinsic parameters, namely ΔH_f and the maximum possible amorphization range, and the model successfully predicted the GFA or GFR of the binary metal systems, which are accordingly classified into three categories of readily, possibly, and hardly glass-forming systems.[3] In recent years, the molecular dynamics (MD) simulation has been proved as a powerful means to study the amorphization transition, especially to understand the underlying physics at an atomic scale. For instance, Zhang and Lai have successfully conducted MD simulations with realistic *n*-body potentials to study the amorphization transition and calculate the GFA or GFR for the Ni-Mo, Ni-Ti, and Ni-Ta systems, which are all characterized with negative ΔH_f.[4–6] Immiscible systems with positive ΔH_f, however, have hardly ever been studied by MD simulations for atomistic modeling, probably due to a formidable obstacle in deriving a realistic *n*-body potential, as there does not exist any equilibrium compound to provide necessary physical properties to fit the cross potentials. In fact, amorphous alloys have been obtained in some immiscible copper-refractory metal systems and the corresponding GFRs have been measured in experiments as well.[7–9] It is therefore desirable to understand the amorphization mechanism at an atomic scale as well as to find out if, or not, the GFA of the immiscible systems could be determined directly by the inter-atomistic potentials through MD simulations.

Among the immiscible copper-refractory metal systems, the Cu-W system has the highest ΔH_f of +33 kJ/mol and is highly immiscible in both solid and liquid states.[10] In the present study, the Cu-W system was selected as a model system, partly due to the potential application of W as a diffusion barrier between Cu and Si/SiO_2 in very large scale integration devices.[11] Accordingly, we first construct an *n*-body potential under an embedded-atom method (EAM) by fitting the cross Cu-W potential to some physical properties, which are obtained from first-principles calculations. Applying the constructed Cu-W potential, MD simulations are then performed with solid solution models to study the amorphization transition and associated property change as well as to determine the GFA of the Cu-W system.

II. CONSTRUCTION OF AN *N*-BODY POTENTIAL

It is well known that the EAM has become one of the most realistic methods to construct *n*-body potentials and is capable of reproducing some physical properties of the transition metals and alloys.[12–14] Consequently, in the present study, the Cu-Cu and W-W potentials take the EAM forms adopted by Cai *et al.* and Johnson *et al.* respectively,[12,13] with some modifications proposed by the present authors:

$$E_{\mathrm{tot}}=\sum_i F_i(\rho_i)+\frac{1}{2}\sum_{\substack{i,j\\(i\neq j)}}\phi_{ij}(r_{ij}), \tag{1}$$

$$F(\rho)=-F_0\left[1-\ln\left(\frac{\rho}{\rho_e}\right)^n\right]\left(\frac{\rho}{\rho_e}\right)^n+F_1\left(\frac{\rho}{\rho_e}\right), \tag{2}$$

$$\rho_i=\sum_{j\neq i} f(r_{ij}), \tag{3}$$

©2003 The American Physical Society

$$f(r)=f_e\exp[-\chi(r/r_e-1)], \tag{4}$$

$$\phi_{\mathrm{Cu}}(r)=-\alpha[1+\beta(r/r_a-1)]\exp[-\beta(r/r_a-1)], \tag{5}$$

$$\phi_{\mathrm{W}}(r)=\begin{cases} k_0+k_1(r/r_e-1)+k_2(r/r_e-1)^2+k_3(r/r_e-1)^3, & r_e\leqslant r\leqslant r_s\\ \phi_{\mathrm{W}}(r)+k_a[\phi_{\mathrm{W}}(r)-\phi_{\mathrm{W}}(r_e)](r/r_e-1)^2, & r\leqslant r_e, \end{cases} \tag{6}$$

where E_{tot} is the total energy, $F(\rho)$ is the embedding energy, ρ_i is the total electron density at atom i due to all other atoms, $\phi(r_{ij})$ is the pair potential between atom i and j, and $f(r_{ij})$ is the electron density for atom i contributed by atom j. For simplicity, the $f(r)$ of the W-W potential in the present study takes the same function form [shown in Eq. (4)] as that of the Cu-Cu potential, and it is different from the original form proposed by Johnson *et al.*[13] In Eq. (2), F_0, ρ_e, and n are three constants. $F_0=E_c-E_v^f$, in which E_c and E_v^f are the cohesive energy and vacancy formation energy, respectively. The parameter ρ_e represents the host electron density at an equilibrium state and the constant n, in the present study, is set to be 0.333333 and 0.440653 for the Cu-Cu and W-W potentials, respectively. For W with a bcc structure, F_1 equals 0. While for Cu of an fcc structure, F_1 is an adjustable parameter. In Eq. (4), r_e is an equilibrium first-neighbor distance, and f_e is a scaling factor determined by the relationship of $f_e=E_c/\Omega$, where Ω is the atomic volume. In Eq. (6), k_a is a constant and is expressed by

$$k_a=4.5\{1+4/[2C_{44}(C_{11}-C_{12})-0.1]\}. \tag{7}$$

The cutoff function is adopted from the polynomial proposed by Guellil *et al.*[14] and the cutoff distances are assumed to be between the second- and third-neighbor distances for Cu-Cu and W-W, respectively. In the above equations, there are totally five parameters $(\chi,\alpha,\beta,r_a,F_1)$ to be fitted for the Cu-Cu potential and also five parameters (χ,k_0,k_1,k_2,k_3) to be fitted for the W-W potential.

The Cu-W cross potential takes a linear combination of the Cu-Cu and W-W potentials, which is the same function proposed by the authors while constructing the cross Cu-Ta potential:[15]

$$\phi_{\mathrm{CuW}}(r)=A[\phi_{\mathrm{Cu}}(r+B)+\phi_{\mathrm{W}}(r+C)], \tag{8}$$

where r is the distance between Cu and W atoms. A, B, and C are three potential parameters to be fitted. It should be pointed out that the fitting of the Cu-W cross potential is a challenging issue, as in the immiscible Cu-W system there is no any equilibrium alloy phase and therefore no indispensable data available for fitting the cross potential. In this respect, the first-principles calculation based on quantum mechanics is a reliable way for attaining some physical properties of the equilibrium as well as nonequilibrium alloy phases.[15,16] We, therefore, performed first-principles calculations, based on the well-established Vienna *ab initio* simulation package (VASP),[17] to obtain the cohesive energies and lattice constants of two nonequilibrium CuW and $\mathrm{Cu_3W}$ alloy phases in the Cu-W system. Briefly, the establishment of the VASP code was based on the density functional theory within the local-density approximation. The electron-ion interaction was described by pseudopotentials and the method used to build the pseudopotentials was derived from Vanderbilt's recipe previously employed for ultrasoft pseudopotentials.[18] The pseudopotentials allowed the use of a moderate cutoff for the construction of the plane-wave basis for the transition metals. The integration in the Brillouin zone was done on some special points in the reciprocal *k*-space determined by employing the Monkhorst-Pack scheme.[19] All calculations were performed with the generalized-gradient approximation proposed by Perdew and Wang.[20] Accordingly, Fig. 1 exhibits the calculated total energy versus average atomic volume for the nonequilibrium $\mathrm{Cu_3W}$ phase with four selected structures of $A15$, $L1_2$, $L6_0$, and $D0_9$, respectively. It can be seen that the $\mathrm{Cu_3W}$ with a $L1_2$ structure could be relatively stable. Meanwhile, similar calculations indicate that the nonequilibrium CuW phase with a $B2$ structure shows a relatively low energy, compared with other possible structures (calculated curves not shown). As a result, the cohesive energies of the $L1_2$ $\mathrm{Cu_3W}$ and $B2$ CuW phases are 4.2478 and 5.4765 eV/atom, respectively, and their lattice constants are 3.76 and 3.04 Å, respectively. The computed data are then applied in fitting the Cu-W cross potential.

After the fitting procedure and optimization of the potential parameters, Table I lists the fitted parameters for the Cu-

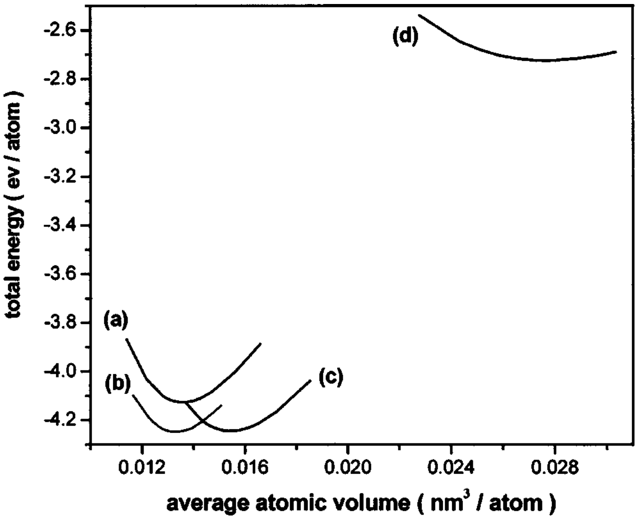

FIG. 1. The *ab initio* calculated total energy vs the average atomic volume for the nonequilibrium $\mathrm{Cu_3W}$ phase with the possible structures of (a) $A15$, (b) $L1_2$, (c) $L6_0$ ($c/a=0.863$), and (d) $D0_9$, respectively.

TABLE I. Fitted parameters for the Cu-Cu, W-W, and Cu-W potentials. The cutoff distances, r_s (Å) and r_c (Å), are also listed.

Cu-Cu		W-W		Cu-W	
χ	11.134 231	χ	6.180 480	A	0.362 635
α (eV)	0.725 977	k_0 (eV)	−0.581 958		
β	3.457 434	k_1 (eV)	−2.175 060	B (Å)	−0.229 870
r_a (Å)	1.629 356	k_2 (eV)	17.053 662		
F_1 (eV)	0.676 073	k_3 (eV)	−8.215 108	C (Å)	0.094 444
r_s (Å)	3.7	r_s (Å)	3.2		
r_c (Å)	4.4	r_c (Å)	4.4		

Cu, W-W, and Cu-W potentials, as well as the cutoff distances of r_s and r_c for the Cu-Cu and W-W potentials, respectively. Table II shows a comparison between some physical properties reproduced by the constructed potentials and experimental/*ab initio* values used initially for fitting the potentials. It can be seen that the constructed Cu-Cu potential shows a better description of the pure Cu than that of the original potential proposed by Cai *et al.*,[12] and the constructed W-W potential gives the better results in reproducing some physical properties of the pure W than those obtained by Mehl *et al.* employing the total-energy tight-binding potential.[22] Evidently, the constructed Cu-W potentials work fairly well in terms of reproducing some physical properties of the pure Cu and W, as well as two nonequilibrium Cu_3W and CuW phases in the system.

III. SIMULATION MODEL AND CHARACTERIZATION METHODS

In the present study, we adopt an fcc solid solution model, which is set to consist of $7\times7\times7\times4=1372$ atoms in a fcc structure. In the model, the [100], [010], and [001] atomic crystal directions are parallel to the *x*, *y*, and *z* axes, respectively and periodic boundary conditions are adopted in three dimensions.

Employing the constructed Cu-W potential, MD simulations with the fcc solid solution model are carried out with Parrinello-Rahman constant pressure scheme and the equations of motion are solved through a fourth-order predictor-corrector algorithm of Gear with a time step $t=5\times10^{-15}$ s.[23] To simulate the Cu-W solid solutions, the initial fcc solid solution model is obtained by randomly substituting a certain amount of Cu by W atoms in the original lattice. The solid solution model is then run at a constant temperature 300 K to reach a relatively equilibrium state, at which all the dynamic parameters show no secular variation. The amount of W solute atoms is gradually increased to find out the critical compositions, at and beyond which the solid solutions would become energetically unstable and collapse into the corresponding disordered states.

The process of solid-state crystal-to-amorphous transition in the model is monitored by the projections of the atomic positions, the planar structure factor $S\,(\mathbf{k},\mathbf{z})$, the pair-correlation function $g(r)$, as well as the density profiles of each species along the *z* direction $\rho_\alpha(z)$. $S\,(\mathbf{k},\mathbf{z})$ is a Fourier transformation of the density in each crystallographic plane

TABLE II. Comparison between calculated values and experimental data/*ab initio* results of the cohesive energy E_c (eV), lattice constant a (Å), elastic constants (Mbar), and vacancy formation energy E_v^f (eV) in the Cu-W system.

Structure			E_c (eV)	a (Å)	C_{11} (Mbar)	C_{12} (Mbar)	C_{44} (Mbar)	E_v^f (eV)
		Experimental	3.54[a]	3.615[a]	1.70[a]	1.225[a]	0.758[a]	1.30[a]
Cu	fcc	Cais[a]	3.52	3.615	1.68	1.263	0.752	1.31
		This work	3.54	3.615	1.70	1.225	0.758	1.30
		Experimental	8.66[b]	3.16475[b]	5.326[c]	2.05[c]	1.631[c]	3.95[c]
W	bcc	Mehls[d]		3.14	5.29	1.70	1.98	6.43
		This work	8.66	3.16475	5.326	2.05	1.63	3.95
Cu_3W	$L1_2$	*Ab initio*	4.2478	3.76				
		Fitted	4.2112	3.728				
CuW	$B2$	*Ab initio*	5.4765	3.04				
		Fitted	5.3920	3.047				

[a] Reference 12.
[b] Reference 13.
[c] Reference 21.
[d] Reference 22.

parallel to the *x-y* plane. Accordingly, the planar structure factor $S=1$ refers to an entirely ordered crystal, while $S=0$ is for a completely disordered state.[24] As one of the main criteria to determine an amorphous structure, $g(r)$ is commonly used to identify the structure of a block material by sampling the atoms involved in the block.[25] $\rho_\alpha(z)$ is calculated to define the position of a single atomic layer, indicating the local structural and compositional properties of the models.[26]

IV. RESULTS AND DISCUSSION

Based on extensive data concerning the amorphous alloy formation by various techniques, Liu *et al.* have proposed to define the experimentally determined GFR as the nominal GFR, for it depends on the specific applied producing technique, e.g., by using the liquid melt quenching technique, the faster the cooling speed, the broader the GFR.[27] From a physical point of view, however, a binary metal system should have its own GFA or GFR, which has nothing to do with the practically applied producing technique, as the atomic configuration corresponding to a disordered state is determined by its intrinsic characteristics. Naturally, such a GFA or GFR is therefore considered as an intrinsic one. In principle, the nominal GFR is frequently smaller than the intrinsic GFR and, apparently, the greater the GFR observed by a specific technique, the closer the nominal GFR to the intrinsic GFR. It has been proved that ion beam mixing is one of the most powerful techniques in producing amorphous alloys and that in the binary metal systems, amorphous alloys, namely, metallic glasses, could be formed within a broad composition range, extending from the central portion to the edges, where the formation of solid solutions of simple crystalline structures becomes energetically more favored than a disordered state. A scientific issue of determining the intrinsic GFR of a system is thus transferred to an objective by comparing the energetic levels of a disordered state versus the solid solution as a function of alloy composition to determine the critical solid solubility. The composition range bounded by the two terminal solubility limits is therefore the intrinsic GFA or GFR of the system.[28] For the Cu-W system, solid solution models are therefore used in MD simulations based on the newly constructed Cu-W potential and the intrinsic GFA or GFR is determined to be within 20–65 at. % of W, which is in good agreement with experimental observations reported in the literature.

We now discuss in detail the results obtained by MD simulations. As a typical example to show the determination of the critical composition, Figure 2 exhibits the projections of atomic positions of $Cu_{35}W_{65}$ and $Cu_{30}W_{70}$ solid solutions after annealing at 300 K for 0.5 ns, respectively. It can be seen vividly that a uniform disordered structure is formed in the $Cu_{35}W_{65}$ solid solution model, while the $Cu_{30}W_{70}$ solid solution still remains in an ordered state, indicating that 35 at. % Cu or 65 at. % W is the critical composition to trigger amorphization transition. Besides, the structural change during annealing was monitored by the partial and total pair-correlation functions, which are considered as the decisive measure to confirm a disordered state and displayed in Fig. 3. Apparently, it can be deduced from Fig. 3 that after annealing at 300 K for 0.5 ns, the $Cu_{85}W_{15}$ and $Cu_{30}W_{70}$ solid solutions still remain in crystalline structures, while the $Cu_{80}W_{20}$, $Cu_{50}W_{50}$, and $Cu_{35}W_{65}$ solid solutions all become amorphous, indicating that 20 at. % of W and 65 at. % of W, are two critical compositions for amorphization transition in the Cu-W system. Furthermore, Fig. 4 shows the calculated density profiles, $\rho_\alpha(z)$, of Cu and W atoms along the *z* direction in $Cu_{85}W_{15}$, $Cu_{80}W_{20}$, $Cu_{50}W_{50}$, $Cu_{35}W_{65}$, and $Cu_{30}W_{70}$ solid solutions after annealing at 300 K for 0.5 ns, respectively. It should be noticed that a relatively uniform distributed density profile $\rho_\alpha(z)$ is achieved only when the alloy composition is in the range of 20–65 at. % of W, providing supplemental evidence to the above determined two critical compositions in the Cu-W system. It follows that the GRF of the Cu-W system is from 20 to 65 at. % of W.

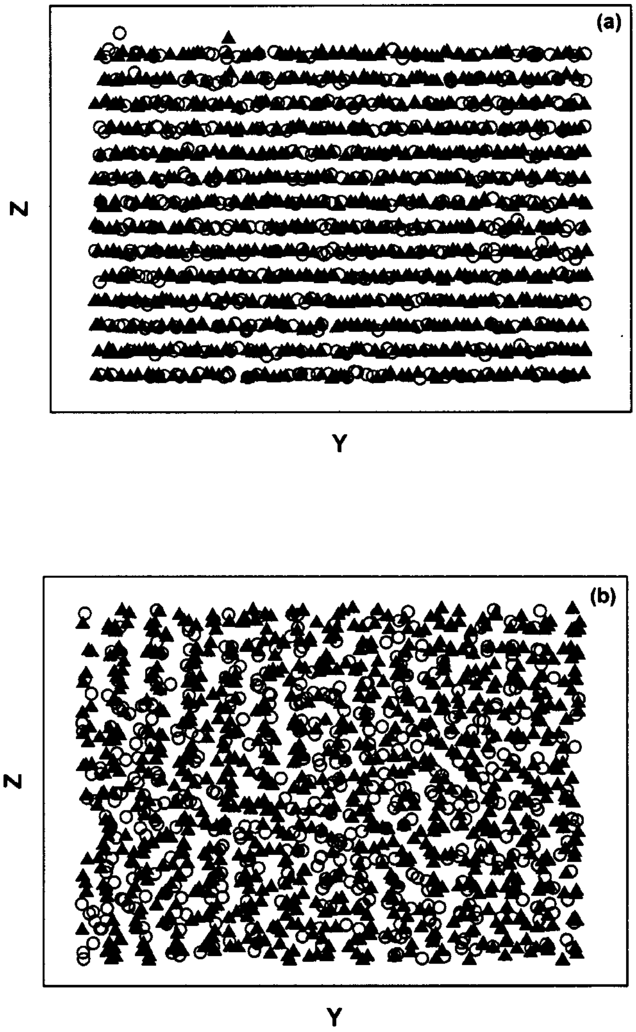

FIG. 2. The projections of atomic positions of (a) $Cu_{30}W_{70}$ and (b) $Cu_{35}W_{65}$ solid solutions after annealing at 300 K for 0.5 ns, respectively. Open circles: Cu. Filled triangles: W.

It is of interest to compare the above simulation results with the experimental observations. Rizzo *et al.* claimed that the vapor-deposited Cu-W alloys containing 25–55 at. % W became completely amorphous.[9] It should be noted that this

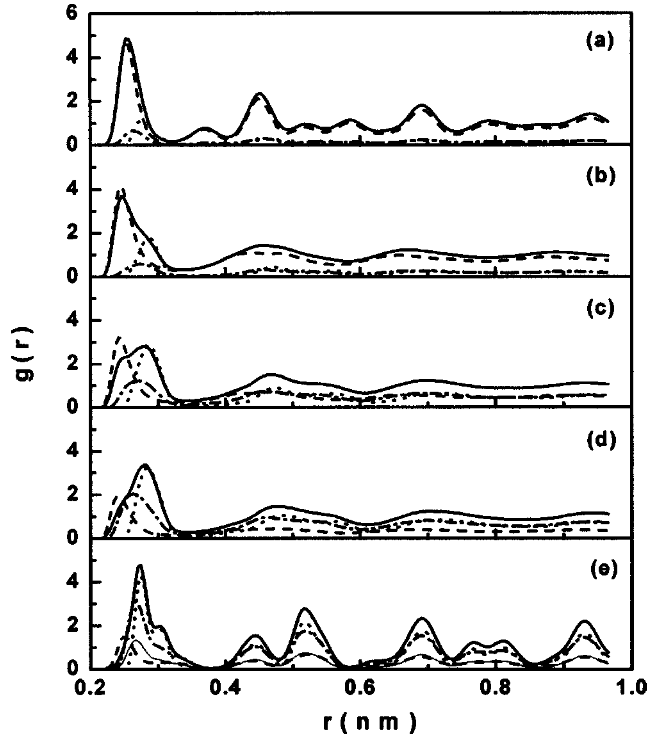

FIG. 3. Partial and total pair correlation functions of (a) $Cu_{85}W_{15}$, (b) $Cu_{80}W_{20}$, (c) $Cu_{50}W_{50}$, (d) $Cu_{35}W_{65}$, and (e) $Cu_{30}W_{70}$ solid solutions after annealing at 300 K for 0.5 ns, respectively. The solid line is for the total $g(r)$, the dashed line is for Cu-Cu partial $g(r)$, the dotted line is for the W-W partial $g(r)$, and the dash-dotted line is for the Cu-W partial $g(r)$.

nominal GFR observed from experiments is very close to, and reasonably a little smaller than the intrinsic value of 20–65 at. %W derived by the present MD simulations. Based on x-ray diffraction and differential thermal analysis, Gaffet *et al.* found that after ball milling, the $Cu_{70}W_{30}$, $Cu_{60}W_{40}$, $Cu_{50}W_{50}$, $Cu_{45}W_{55}$, and $Cu_{40}W_{60}$ alloys became amorphous, whereas the $Cu_{95}W_5$, $Cu_{90}W_{10}$, and $Cu_{85}W_{15}$ alloys retained ordered structures.[29] Gržeta *et al.* reported that the magnetron-sputtered $Cu_{50}W_{50}$ and $Cu_{66}W_{34}$ were in the amorphous states.[30] Obviously, these experimental observations are also in good agreement with the present MD simulation results, as the alloy compositions, i.e., $Cu_{70}W_{30}$, $Cu_{66}W_{34}$, $Cu_{60}W_{40}$, $Cu_{50}W_{50}$, $Cu_{45}W_{55}$, and $Cu_{40}W_{60}$, are all within the presently calculated GFR of 20–65 at. % of W, whereas $Cu_{95}W_5$, $Cu_{90}W_{10}$, and $Cu_{85}W_{15}$ are all out off the calculated GFR. In addition, Chen *et al.* discovered that the structure of the $Cu_{84}W_{16}$ multilayers upon annealing at around 350 °C for about 0.5 h kept still in crystalline fcc,[31] which is also consistent with the present simulation results. In summary, the GFR determined directly by the Cu-W potential through MD simulation is of relevance, which in turn confirms the newly constructed Cu-W potential is realistic as well.

We now turn to determine the volume expansion (ΔV) in association with the amorphization transition in the immiscible Cu-W system. We first calculate, according to Vegard's law, the volume of the Cu-W solid solution after substituting with various compositions of W solute atoms, and regard these values (V_i), rather than the original volume of the pure Cu lattice, as the initial volume of the solid solution. We then define $\Delta V=(V_f-V_i)/V_i$ to describe the actual volume expansion, where V_f is the final volume of the solid solution

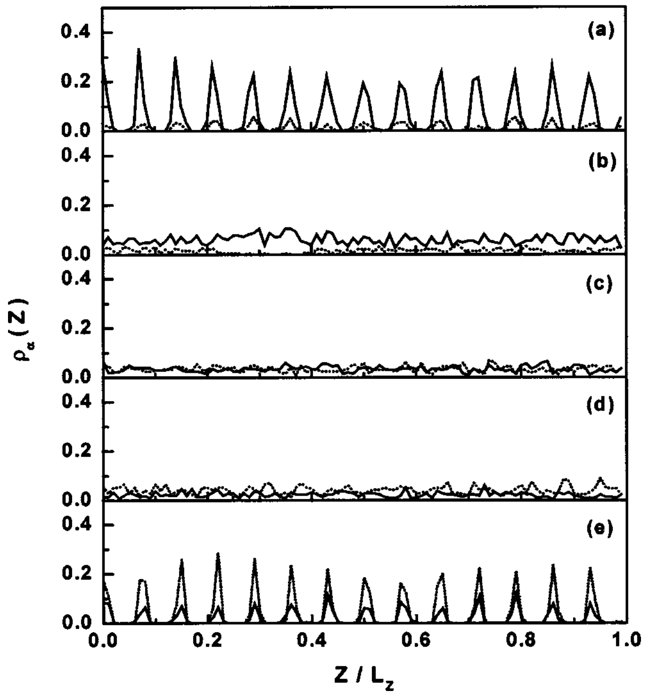

FIG. 4. The calculated density profiles $\rho_\alpha(z)$ of Cu and W atoms along the z direction in (a) $Cu_{85}W_{15}$, (b) $Cu_{80}W_{20}$, (c) $Cu_{50}W_{50}$, (d) $Cu_{35}W_{65}$, and (e) $Cu_{30}W_{70}$ solid solutions after annealing at 300 K for 0.5 ns, respectively. $\rho_{Cu}(z)$ is represented by the solid line and $\rho_W(z)$ by the dotted line. The ordinate is in arbitrary units.

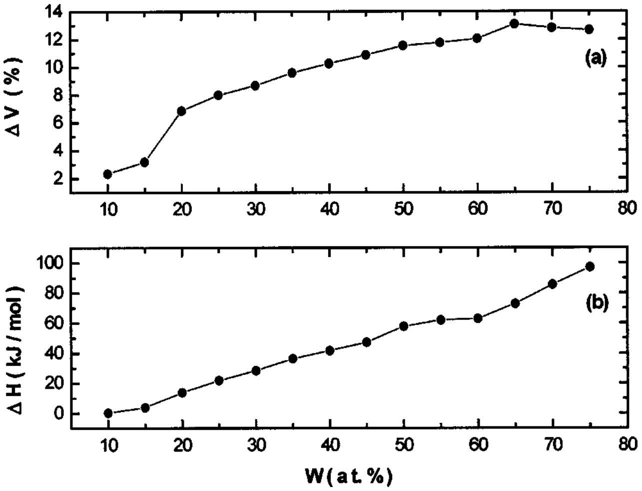

FIG. 5. The actual volume expansion (ΔV) and molar enthalpy change (ΔH) vs the W solute composition in the Cu-W solid solutions. $\Delta V=(V_f-V_i)/V_i$, where V_i is the calculated volume of the solid solution according to Vegard's law and V_f is the final volume of the solution after annealing at 300 k for 0.5 ns. H_i and H_f are the enthalpies of the initial and final states of the Cu-W solid solution after annealing at 300 K for 0 and 0.5 ns, respectively. The enthalpy change is presented by $\Delta H=H_i-H_f$.

after annealing at 300 K for 0.5 ns. Figure 5 exhibits the actual volume expansion (ΔV) as well as the enthalpy change (ΔH) of the Cu-W solid solution as a function of alloy composition. The enthalpy change is expressed by $\Delta H = H_i - H_f$, in which H_i and H_f are the enthalpies of the initial and final states, corresponding to annealing at 300 K for 0 and 0.5 ns, respectively. It can be seen that ΔV and ΔH increase with increasing of the W solute concentration, and at $x_W = 20$ and 65 at. %, the slopes of the enthalpy and volume expansion are discontinuous, giving additional evidence to the calculated GFR of the Cu-W system. As shown in Fig. 5, the actual volume expansion in association with the amorphization transition in the immiscible Cu-W system is from 6.9 % to 13.1 %, which is surprisingly greater than the typical value of 1–2 % usually observed in the binary metal systems with negative ΔH_f.[32,33] From a physical point of view, such a large volume expansion upon the amorphization transition reflects the repulsive interaction between the Cu and W atoms, which is revealed by the newly constructed *n*-body Cu-W potential in the present study, and is compatible with a large positive ΔH_f of the system characterized from the thermodynamic calculation.

V. CONCLUSIONS

We have shown that the *ab initio* calculation is a unique means to provide some physical properties of the nonequilibrium Cu_3W and CuW phases for fitting the Cu-W cross potential and consequently, a realistic EAM Cu-W potential is constructed for the highly immiscible Cu-W system. Based on the potential, it is determined through molecular dynamics simulations that the intrinsic glass-forming range of the Cu-W system is from 20 to 65 at. % of W, which is in good agreement with the experimental observations. In addition, the volume expansion in association with the amorphization transition is from 6.9% to 13.1%, which is unusually large probably due to the repulsive interaction between the Cu and W atoms.

ACKNOWLEDGMENTS

The authors are grateful for the financial support from the National Natural Science Foundation of China, The Ministry of Science and Technology of China (G20000672), as well as from Tsinghua University.

---

*Author to whom correspondence should be addressed. Electronic mail: dmslbx@tsinghua.edu.cn

[1] B. X. Liu, W. L. Johnson, M.-A. Nicolet, and S. S. Lau, Appl. Phys. Lett. **42**, 45 (1983).
[2] J. A. Alonso and S. Simozar, Solid State Commun. **48**, 765 (1983).
[3] B. X. Liu, E. Ma, J. Li, and L. J. Huang, Nucl. Instrum. Methods Phys. Res. B **19/20**, 682 (1987).
[4] Q. Zhang, W. S. Lai, and B. X. Liu, Phys. Rev. B **59**, 13 521 (1999).
[5] W. S. Lai, Q. Zhang, B. X. Liu, and E. Ma, J. Phys. Soc. Jpn. **69**, 2923 (2000).
[6] Q. Zhang, W. S. Lai, and B. X. Liu, Phys. Rev. B **61**, 9345 (2000).
[7] J. H. Kim, H. Yoshioka, H. Habazaki, A. Kawashima, K. Asami, and K. Hashimoto, Mater. Sci. Eng., A **156**, 211 (1992).
[8] E. Hirota, H. Yoshioka, H. Habazaki, A. Kawashima, K. Asami, and K. Hashimoto, Corros. Sci. **32**, 1213 (1991).
[9] H. F. Rizzo, T. B. Massalski, and M. Nastasi, Metall. Trans. A **24**, 1027 (1993).
[10] F. R. de Boer, R. Boom, W. C. M. Mattens, A. R. Miedema, and A. K. Niessen, *Cohesion in Metals: Transition Metal Alloys* (North-Holland, Amsterdam, 1989).
[11] L. T. Kong, X. Y. Li, W. S. Lai, J. B. Liu, and B. X. Liu, Jpn. J. Appl. Phys. **41**, 4503 (2002).
[12] J. Cai and Y. Y. Ye, Phys. Rev. B **54**, 8398 (1997).
[13] R. A. Johnson and D. J. Oh, J. Mater. Res. **4**, 1195 (1989).
[14] A. M. Guellil and J. B. Adams, J. Mater. Res. **7**, 639 (1992).
[15] H. R. Gong, L. T. Kong, W. S. Lai, and B. X. Liu, Phys. Rev. B **66**, 104204 (2002).
[16] F. Ercolessi and J. B. Adams, Europhys. Lett. **26**, 583 (1994).
[17] G. Kresse and J. Hafner, Phys. Rev. B **47**, 558 (1993).
[18] D. Vanderbilt, Phys. Rev. B **41**, 7892 (1990).
[19] H. J. Monkhorst and J. D. Pack, Phys. Rev. B **13**, 5188 (1976).
[20] J. Perdew and Y. Wang, Phys. Rev. B **45**, 13 244 (1992).
[21] B. J. Lee, M. I. Bakes, H. Kim, and Y. K. Cho, Phys. Rev. B **64**, 184102 (2001).
[22] M. J. Mehl and D. A. Papaconstantopoulos, Phys. Rev. B **54**, 4519 (1996).
[23] M. Parrinello and A. Rahman, J. Appl. Phys. **52**, 7182 (1981).
[24] S. R. Phillpot, S. Yip, and D. Wolf, Comput. Phys. **3**, 20 (1989).
[25] Y. Waseda, *The Structure of Non-Crystalline Materials: Liquid and Amorphous Solids* (McGraw-Hill, New York, 1980).
[26] V. Rosato, G. Ciccotti, and V. Pontikis, Phys. Rev. B **33**, 1860 (1986).
[27] B. X. Liu, W. S. Lai, and Q. Zhang, Mater. Sci. Eng., R. **29**, 1 (2000).
[28] B. X. Liu, W. S. Lai, and Z. J. Zhang, Adv. Phys. **50**, 367 (2001).
[29] E. Gaffet, C. Louison, M. Harmelin, and F. Faudot, Mater. Sci. Eng., A **134**, 1380 (1991).
[30] B. Gržeta, N. Radić, D. Gracin, T. Došlić, and T. Car, J. Non-Cryst. Solids **170**, 101 (1994).
[31] Y. G. Chen and B. X. Liu, J. Phys. D **30**, 1729 (1997).
[32] M. Li and W. L. Johnson, Phys. Rev. Lett. **70**, 1120 (1993).
[33] D. Wolf, P. R. Okamoto, S. Yip, J. F. Lutsko, and M. Kluge, J. Mater. Res. **5**, 286 (1990).